Development 139, 4007-4019 (2012) doi:10.1242/dev.081703

Cooperative and antagonistic roles for Irx3 and Irx5 in cardiac morphogenesis and postnatal physiology

Nathalie Gaborit[1], Rui Sakuma[2], John N. Wylie[1], Kyoung-Han Kim[2], Shan-Shan Zhang[1], Chi-Chung Hui[2,3] and Benoit G. Bruneau[1,4,5,*]

SUMMARY

The Iroquois homeobox (Irx) homeodomain transcription factors are important for several aspects of embryonic development. In the developing heart, individual Irx genes are important for certain postnatal cardiac functions, including cardiac repolarization (*Irx5*) and rapid ventricular conduction (*Irx3*). Irx genes are expressed in dynamic and partially overlapping patterns in the developing heart. Here we show in mice that *Irx3* and *Irx5* have redundant function in the endocardium to regulate atrioventricular canal morphogenesis and outflow tract formation. Our data suggest that direct transcriptional repression of *Bmp10* by Irx3 and Irx5 in the endocardium is required for ventricular septation. A postnatal deletion of *Irx3* and *Irx5* in the myocardium leads to prolongation of atrioventricular conduction, due in part to activation of expression of the Na^+ channel protein Nav1.5. Surprisingly, combined postnatal loss of *Irx3* and *Irx5* results in a restoration of the repolarization gradient that is altered in *Irx5* mutant hearts, suggesting that postnatal Irx3 activity can be repressed by Irx5. Our results have uncovered complex genetic interactions between *Irx3* and *Irx5* in embryonic cardiac development and postnatal physiology.

KEY WORDS: Transcription factors, Heart development, Electrophysiology, Mouse

INTRODUCTION

Heart development is governed by a complex network of transcription factors that precisely regulates cardiac gene expression (Olson, 2006; Srivastava, 2006; Evans et al., 2010). Many transcription factors are specifically expressed in cardiogenic tissue early in development and are required for early steps in cardiogenesis. These factors are also relevant to human diseases, as mutations in these genes are associated with human congenital structural heart defects, including defects in chamber septation and outflow tract formation (Bruneau, 2008). No single transcription factor has been shown to be essential for all aspects of cardiogenesis, which is likely to reflect considerable functional redundancy between transcription factors in the cardiac lineage.

Transcription factors of the Iroquois homeobox (Irx) family are expressed in the heart and have conserved roles during embryonic development in metazoans (Christoffels et al., 2000; Cavodeassi et al., 2001; Mummenhoff et al., 2001). In mouse, five out of the six Irx members have been individually deleted, and deletions of three result in defects of cardiac function. *Irx4*-deficient mice develop adult mild cardiomyopathy and abnormal ventricular gene expression (Bruneau et al., 2001). Deletions of *Irx3* or *Irx5* lead to specific defects in adult ventricular conduction or repolarization, respectively (Costantini et al., 2005; Zhang, S. S. et al., 2011). The Irx genes encode proteins of similar structure, containing a highly conserved DNA-binding homeodomain, followed by an acidic activation domain and the IRO (Iroquois) box, a conserved motif of unknown function (Burglin, 1997). Irx genes provide a rare example of genetic redundancy in *Drosophila* (Gomez-Skarmeta et al., 1996; Cavodeassi et al., 2001) and are highly redundant in zebrafish (Itoh et al., 2002). Murine Irx genes are expressed in partially overlapping patterns in most developing tissues and organs, including the heart (Christoffels et al., 2000; Houweling et al., 2001; Mummenhoff et al., 2001). Although *Irx3* or *Irx5* deletion does not lead to abnormalities in embryonic cardiac morphogenesis (Costantini et al., 2005; Zhang, S. S. et al., 2011), the Fused toes mouse, in which three Irx genes (*Irx3*, *Irx5* and *Irx6*) are deleted, displays cardiac abnormalities in utero (Peters et al., 2002). Along with the protein homology of the Irx3 and Irx5 transcription factors and their overlapping expression patterns, these data suggest that they function redundantly in pre-natal cardiac development as well as postnatal cardiac function.

To investigate the potential functional redundancy between *Irx3* and *Irx5*, we generated mice bearing a deletion of both genes. In contrast to the single knockouts, mice lacking both *Irx3* and *Irx5* die in utero and have severe defects of the outflow tract (OFT) and atrioventricular (AV) canal due to specific requirement for *Irx3* and *Irx5* in the endocardium. Several BMPs are upregulated in the embryonic double-knockout (DKO) mice, *Bmp10* being a direct downstream target of repression by Irx3 and Irx5. In addition, we analyzed the postnatal redundancy of *Irx3* and *Irx5* in the cardiac conduction system by generating a postnatal deletion of both genes in the cardiac tissue. The spectrum of electrophysiological defects in these mice suggests redundant and unique roles for Irx3 and Irx5 in the conduction of the ventricular electrical influx. These results reveal new and partially redundant roles for *Irx3* and *Irx5* during heart development and postnatal function.

MATERIALS AND METHODS

Gene targeting and mice

Generation of the $Irx3^{flox}$ $Irx5^{EGFP}$/$Irx3^{flox}$ $Irx5^{EGFP}$ mice was achieved by sequential gene targeting in embryonic stem cells (R.S. and C.-C.H., unpublished). Briefly, a conditional allele for *Irx3* was generated by

[1]Gladstone Institute of Cardiovascular Disease, San Francisco, CA 94158, USA. [2]Program in Developmental & Stem Cell Biology, The Hospital for Sick Children, Toronto, ON M5G 1X8, Canada. [3]Department of Molecular Genetics, University of Toronto, Toronto, ON M5S 3E2, Canada. [4]Cardiovascular Research Institute, University of California, San Francisco, San Francisco, CA 94158, USA. [5]Department of Pediatrics, University of California, San Francisco, San Francisco, CA 94143, USA.

*Author for correspondence (bbruneau@gladstone.ucsf.edu)

Accepted 31 July 2012

flanking exons 2 to 4 with loxP sites. This line was then retargeted to replace *Irx5* exon 1 by *EGFP* cDNA, followed by a polyadenylation signal sequence. A PGK-puro cassette was also introduced in place of *Irx5* exon 2, thereby deleting the homeobox domain. Genotyping was carried out using the following primers (5′-3′): $Irx3^{flox}$ allele, CAAGAAGGGGTGATGAGAGTCGCTGGGCG and GGAGAGGGAACCACGGCGAGAAAGGCCTA; $Irx3^{KO}$ allele, CTCGGATACCAGTACATCCGCCCTCTCTA and GGAGAGGGAACCACGGCGAGAAAGGCCTA; $Irx5^{EGFP}$ allele, GGTCCCGAAGGGCCAGAATCAGAATTGGGG, GCATTCTTCCGGTACGCGGGGTCCCCATA and CCGGTGGATGTGGAATGTGTGCGAGGCCA. Complete deletion of *Irx3* was obtained by crossing with *Mef2cAHF::Cre* female mice, which have germline Cre activity (Verzi et al., 2005). $Irx3^{TaulacZ}$, *Wnt1::Cre*, *Mef2cAHF::Cre*, *Nkx2.5::Cre*, *Tie2::Cre*, *Isl1::Cre*, *Myh6::MerCreMer* and *ca-Bmpr1a* have been described (Brault et al., 2001; Kisanuki et al., 2001; Sohal et al., 2001; McFadden et al., 2004; Verzi et al., 2005; Yang et al., 2006; Kamiya et al., 2008; Zhang, S. S. et al., 2011). Animals were cared for in accordance with national and institutional requirements.

Histology

Embryos were harvested from timed matings and fixed in 4% paraformaldehyde (PFA) overnight, followed by embedding in paraffin and staining with Hematoxylin and Eosin (H&E). Optical projection tomography (OPT) imaging of hearts was performed as described (Sharpe et al., 2002; Lickert et al., 2004).

Protein expression analysis

For immunofluorescence analysis, 8 μm cryosections were stained with primary antibodies against β-galactosidase (Cappel), green fluorescent protein (GFP) (Abcam), phospho-Smad1/5/8 (Cell Signaling Technology), Cx40 (Alpha Diagnostic), Nav1.5 (Alomone) and Kv4.2 (Abcam). Secondary antibody staining was performed using Alexa 488- and Alexa 594-conjugated antibodies (Invitrogen). Vectashield Mounting Media with DAPI was used for DNA counterstaining and mounting (Vector Laboratories).

Gene expression analysis

For microarray analysis, ventricles and OFT were dissected from E12.5 hearts and digested with 0.2 mg/ml trypsin (Invitrogen) and 50 U/ml type II collagenase (Worthington) in calcium- and magnesium-free Hanks' buffer with Hepes at 37°C. $Irx5^{EGFP}$-positive cells were isolated using FACSDiva. RNA was isolated using the PicoPure RNA Isolation Kit (Arcturus Bioscience). For each sample, 1 ng RNA was amplified using the FFPE Kit (NuGEN) and hybridized on Mouse Gene ST 1.0 microarrays (Affymetrix). For quantitative (q) real-time RT-PCR, 20 ng amplified cDNA was used. Primers (TaqMan assay, Applied Biosystems) for *Tgfbr3*, *Runx1t1*, *Isl1*, *Fgf10*, *Fgfr2*, *Bmp2*, *Bmp5*, *Bmp10* and *Irx3* were as follows: Mm00803538_m1, Mm00486771_m1, Mm00627860_m1, Mm00433275_m1, Mm01275521_m1, Mm01340178_m1, Mm00432091_m1, Mm01183889_m1 and Mm00500463_m1. β-actin (Mm00607939_s1) was used as internal control (Applied Biosystems). In situ hybridization was performed according to a standard protocol using 10 μm paraffin sections.

Luciferase assays, co-immunoprecipitation and chromatin immunoprecipitation

Transfections and luciferase assays were performed using published methods (Bruneau et al., 2001). Cos7 cells were transfected with 250 ng of each plasmid using Fugene (Roche). Co-immunoprecipitation was performed using the ExactaCruz Kit (Santa Cruz) following the manufacturer's instructions. Primary antibody against Irx5 (Sigma WH0010265M1) was used for immunoprecipitation and antibody against Irx3 (Abcam AB25703) was used for immunoblot analysis. For chromatin immunoprecipitation, chromatin was isolated from wild-type E12.5 and E14.5 hearts, sonicated and incubated with antisera against Irx3 (Abcam AB25703) or Irx5 (Sigma WH0010265M1). DNA fragments were analyzed by custom TaqMan assay for the *Bmp10* promoter: 5′-CTGTGGCAGTTGCACGTACT-3′ and 5′-ATGCTTTTTGGAACCTCGTG-3′.

Electrophysiology

Surface ECG was obtained at 8-10 weeks as described (Bruneau et al., 2001). Telemetry devices (Data Sciences International, St Paul, MN, USA) were implanted dorsally with electrodes in lead II configuration. After 60 hours of recovery post-surgery, data were collected and analyzed using Dataquest A.R.T. (DSI) and Chart (ADInstruments).

Data analysis

Statistical comparisons were performed by Student's *t*-test with $P<0.05$ considered significant. Microarrays were normalized for array-specific effects using Affymetrix Robust Multi-Array (RMA) normalization. Normalized arrays values were reported on a $\log_2$ scale. For statistical analyses, we removed array probesets where no experimental groups had an average $\log_2$ intensity greater than 3.0. Linear models were fitted for each gene using the Bioconductor limma package in R. Moderated *t*-statistics, fold-change and the associated *P*-values were calculated for each gene. To account for testing thousands of genes, we reported false discovery rate (FDR)-adjusted values, calculated using the Benjamini-Hochberg method (Benjamini and Hochberg, 1995). FDR values indicate the expected fraction of falsely declared differentially expressed genes among the total set of declared differentially expressed genes. Two-way hierarchical agglomerative clustering was applied to the gene expression matrix consisting of *Irx3*het, *Irx3*KO;*Irx5*het, *Irx5*KO and *Irx3;Irx5* DKO samples (horizontally) and the 458 statistically differentially expressed genes (vertically). Input consists of replicate expression values for each gene and sample. We applied average linkage clustering with uncentered correlation using Cluster software (Eisen et al., 1998). For each gene, expression values were centered to the median. Clusters were visualized using TreeView software. Microarray data are available in GEO with accession number GSE38826.

RESULTS

Expression pattern of *Irx3* and *Irx5* in the embryonic heart

Irx3 and *Irx5* are expressed in complementary domains, at least up until E12.5 (Christoffels et al., 2000). We analyzed the expression pattern of *Irx3* and *Irx5* at E12.5 and E14.5, with $Irx3^{taulacZ}$ and $Irx5^{EGFP}$ alleles and immunostaining for β-gal and EGFP, to define cell types that express either one of these factors. At E12.5, *Irx3*-expressing cells were detected in the ventricular trabeculae (Fig. 1Aa, arrowheads) and in the interventricular septum, at the level of the bundle of His (BH) and bundle branches (BBs) (Fig. 1Ad). These cells colocalize with a marker of cardiomyocytes, tropomyosin (Fig. 1Ba), but not with the endocardial marker PECAM (Pecam1) (Fig. 1Bb). *Irx5* was detected in PECAM-positive cells lining the ventricular trabeculae and septum (Fig. 1Ab,e,Bc,d, arrowheads) that did not express *Irx3* (Fig. 1Ac,f). In addition, we identified a set of $PECAM^+$ cells lining the AV cushions that coexpressed Irx3 and Irx5 (Fig. 1Af,Bb,d, arrows). Fig. 1C illustrates the expression profile of *Irx3* and *Irx5* at E12.5. By E14.5, coexpression of *Irx3* and *Irx5* broadens to include $tropomyosin^+$ cells of the ventricular trabeculae (Fig. 1Da-c, arrowheads) as well as BH and BBs (Fig. 1Dd-f,Ea,b). Fig. 1F summarizes the expression pattern of Irx3 and Irx5 at E14.5.

Cardiac defects in *Irx3;Irx5* DKO embryos

Irx3 and *Irx5* are located within 600 kb of each other on mouse chromosome 8. To create DKOs, the two genes must be targeted in cis. We used an allele that included a replacement of *Irx5* with *EGFP* and a conditional deletion of *Irx3* by flanking exons 2-4 with loxP sites. Crossing the $Irx3^{flox}$ $Irx5^{EGFP}$/$Irx3^{flox}$ $Irx5^{EGFP}$ to a mouse line that expresses Cre recombinase in the germ line, we obtained heterozygous mice ($Irx3^{+}$ $Irx5^{+}$/$Irx3^{KO}$ $Irx5^{EGFP}$) that were viable and fertile. The mating of these mice did not yield

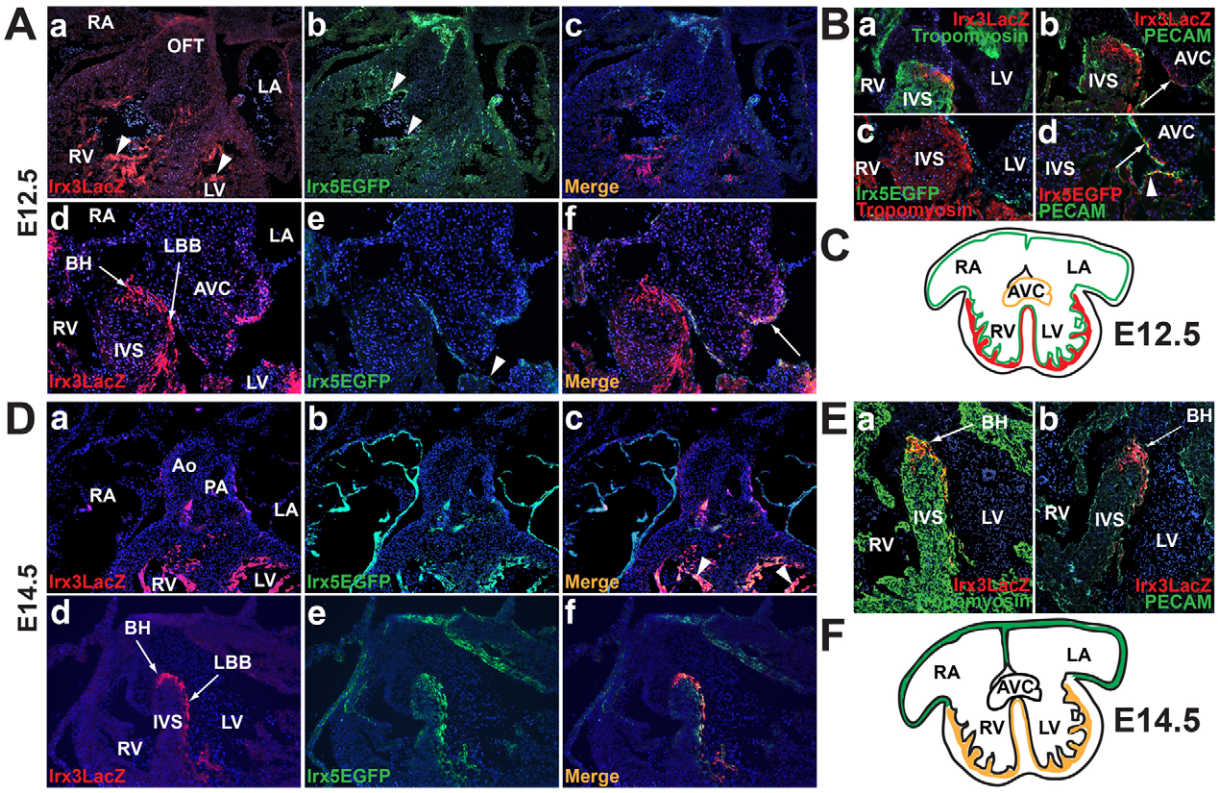

Fig. 1. Expression pattern of *Irx3* and *Irx5* during heart development. (**A-C**) Immunofluorescence colocalization of *Irx3*^{taulacZ} and *Irx5*^{EGFP} expression in the heart of *Irx3*$^{taulacZ/+}$;*Irx5*$^{EGFP/+}$ mouse embryos at E12.5. *Irx3* is uniquely expressed in the myocardium of the trabeculae (arrowheads, Aa) and in the ventricular conduction system (Ad), where it colocalizes with tropomyosin (Ba) but not with PECAM (Bb) or Irx5 (Ac,f). *Irx5* is expressed in the endocardium lining the ventricular septum and trabeculae (arrowheads, Ab,e), where it colocalizes with PECAM (arrowhead, Bd) but not tropomyosin (Bc) or Irx3 (Ac,f). *Irx3* and *Irx5* are coexpressed in the endocardium lining the AV endocardial cushions (arrow, Af) and colocalize at that level with PECAM (arrow, Bb,d). (C) Summary of the expression pattern of *Irx3* and *Irx5* at E12.5. (**D-F**) Immunofluorescence colocalization of *Irx3*^{taulacZ} and *Irx5*^{EGFP} expression in the heart of *Irx3*$^{taulacZ/+}$;*Irx5*$^{EGFP/+}$ embryos at E14.5. *Irx3* and *Irx5* are expressed in the ventricular trabeculae (arrowheads, Da-c) and conduction system, bundle of His (BH) and bundle branches (Dd-f), and they colocalize with tropomyosin (Ea) but not PECAM (Eb). Expression in the atria is restricted to Irx5 (Da-c). (F) Summary of the expression pattern of *Irx3* and *Irx5* at E14.5. RA, right atrium; LA, left atrium; RV, right ventricle; LV, left ventricle; OFT, outflow tract; IVS, interventricular septum; AVC, atrioventricular cushions; LBB, left bundle branch.

homozygous offspring, suggesting that the *Irx3;Irx5* DKO was embryonic lethal. Western blot analysis confirmed the absence of Irx3 and Irx5 proteins in the DKO embryos at E11.5 (R.S. and C.-C.H., unpublished). To determine the onset of embryonic lethality, we collected and genotyped embryos from *Irx3*$^{+}$ *Irx5*$^{+}$/*Irx3*^{KO} *Irx5*^{EGFP} matings at different stages of development. At E14.5, the ratio of the expected genotypes showed normal Mendelian transmission (Table 1). However, from E15.5 onwards, the *Irx3*^{KO} *Irx5*^{EGFP}/*Irx3*^{KO} *Irx5*^{EGFP} genotype was not represented, suggesting lethality of *Irx3;Irx5* DKO embryos after E14.5.

Given that *Irx3* and *Irx5* are coexpressed in the heart and regulate cardiac function, we determined whether embryonic lethality of the *Irx3;Irx5* DKO mice was associated with cardiac structural defects. We produced 3D reconstructions of embryonic hearts by optical projection tomography (OPT) and examined serial transverse sections of wild-type and DKO embryos at several developmental stages. Cardiac malformations were first observed at E11.5. OPT analysis showed an improper orientation of the OFT (Fig. 2A,B). By E12.5, transverse sections revealed a misalignment of the OFT, such that the aorta was abnormally oriented toward the right ventricle (RV) (Fig. 2C,D). Although the growth of the muscular ventricular septum was normal at this stage (Fig. 2E,F), a defect was observed at the level of the atrial septum, with an absence of the dorsal mesenchymal protrusion (DMP) and septum primum (Fig. 2G,H, asterisk). At E14.5, DKO hearts demonstrated an abnormal arrangement of the aorta alongside the pulmonary artery, leading to a double-outlet right ventricle (DORV) (Fig. 2I-L). In addition, we observed a membranous ventricular septal defect (VSD) at the level of the AV canal (Fig. 2M,N, arrowhead) at E12.5, a defect in DMP formation, an atrial septal defect (ASD), and defects in the growth of septa primum and secundum (Fig. 2O,P, asterisk).

Table 1. Lethality of *Irx3;Irx5* DKO embryos after E14.5

Stage	Percentage of embryos of indicated genotype			*n*
	Irx3$^{+/+}$;*Irx5*$^{+/+}$	*Irx3*$^{+/-}$;*Irx5*$^{+/-}$	*Irx3*$^{-/-}$;*Irx5*$^{-/-}$	
E10.5	25	45	30	20
E12.5	24	54	22	50
E14.5	25	53	22	77
E15.5	30	65	4 (resorbed)	23

Percentage of embryos of each genotype at different embryonic stages. At E15.5, *Irx3*$^{-/-}$;*Irx5*$^{-/-}$ embryos were either absent or resorbed (*n*=1) with still enough embryonic material for genotyping. *n*, number of embryos analyzed.

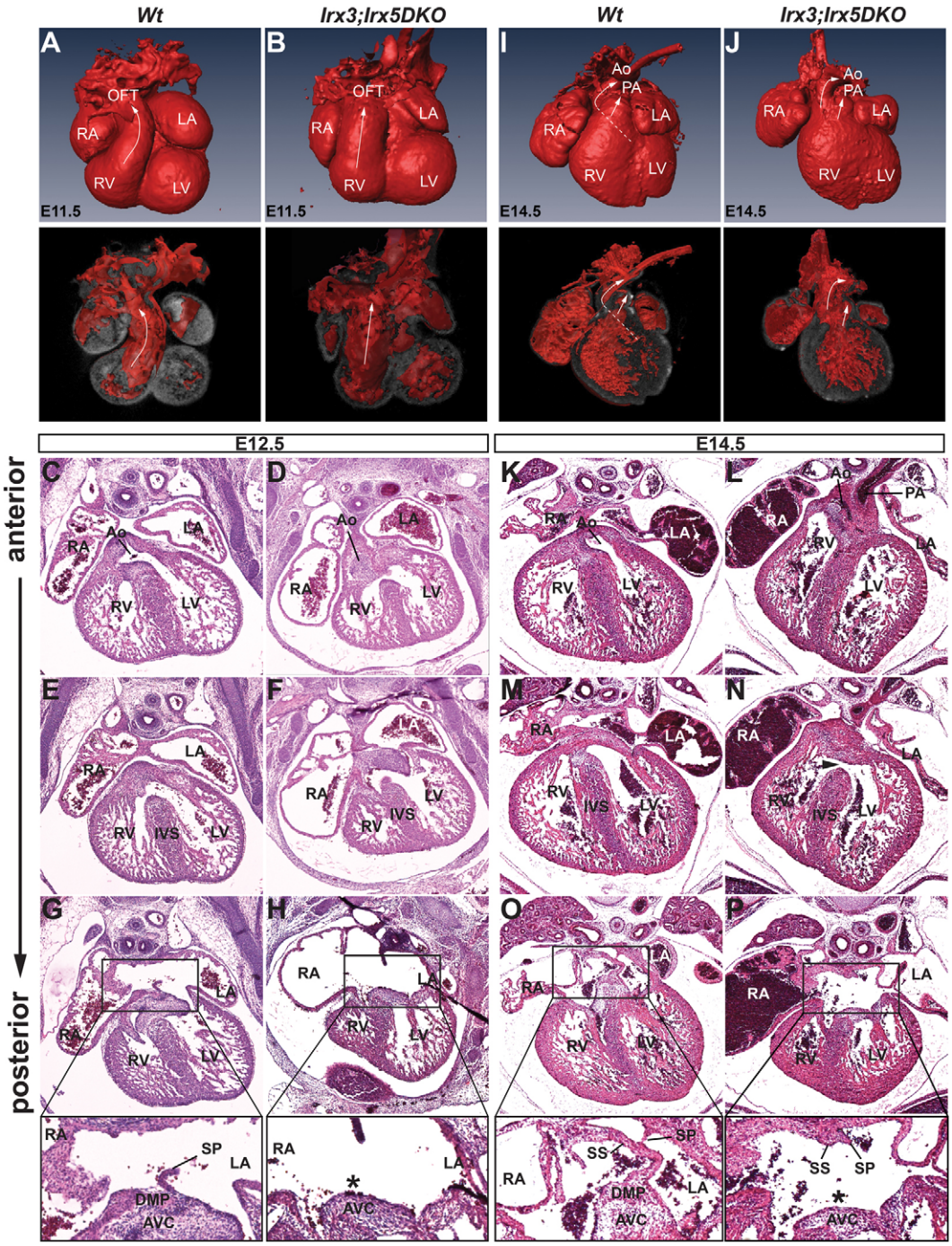

Fig. 2. Abnormal cardiac morphology of *Irx3;Irx5* DKO embryos. (**A**,**B**) Cardiac morphology at E11.5. OPT analysis showing views of the heart surface (top row) and of the inner lumens at the level of the OFT (bottom row) revealing abnormal orientation (arrows) of the OFT in the DKO (*Irx3*^{KO} *Irx5*^{EGFP}/*Irx3*^{KO} *Irx5*^{EGFP}) as compared with the wild-type (*Irx3*$^{+}$ *Irx5*$^{+}$/*Irx3*$^{+}$ *Irx5*$^{+}$) mouse heart. (**C-H**) Cardiac morphology at E11.5. Serial sections with Hematoxylin and Eosin (H&E) staining at the level of the OFT (C,D), showing that the RV and aorta appear to be abnormally aligned. At the level of the AV canal (E-H), the *Irx3;Irx5* DKO embryos have normal growth of the muscular ventricular septum (E,F) but exhibit a defect in atrial septation with absence of the DMP (asterisk, G,H). (**I-P**) Cardiac morphology at E14.5. OPT analysis (I,J) at the surface (top row) and inner lumen (bottom row) as well as sections (K,L) show a double-outlet right ventricle (DORV) in the mutant heart. The dashed line indicates internal path of the aorta. Sections at the level of the AV canal show a membranous ventricular septal defect (arrowhead, M,N) and atrial septation defect with lack of DMP (asterisk, O,P). Genotypes apply to columns. RA, right atrium; LA, left atrium; RV, right ventricle; LV, left ventricle; OFT, outflow tract; Ao, aorta; IVS, interventricular septum; SP, septum primum; DMP, dorsal mesenchymal protrusion; PA, pulmonary artery; SS, septum secundum; AVC, atrioventricular cushions.

These findings demonstrate that *Irx3* and *Irx5* function redundantly in cardiac formation. The location and timing of *Irx3* and *Irx5* activity required for OFT development are not known. Although it is unclear whether the morphological defects alone result in lethality, altered cardiac function is a possible contributing factor.

Cardiac morphogenesis requires endocardial *Irx3* and *Irx5* expression

Our data demonstrate that *Irx3* and *Irx5* are coexpressed in myocardial and endocardial cells at different embryonic stages. In addition, they might also be expressed in cardiac neural crest cells (Houweling et al., 2001). To determine the cellular origin of the DKO heart defects, we deleted *Irx3* in each of these cardiac subdomains, in the background of an *Irx5* deletion. We employed the cis-targeted alleles of $Irx3^{flox}\ Irx5^{EGFP}/Irx3^{flox}\ Irx5^{EGFP}$ to delete *Irx3* conditionally with different Cre-expressing mouse lines, and compared the phenotypes at the level of the OFT and AV canal, with those of $Irx3^{+}\ Irx5^{+}/Irx3^{+}\ Irx5^{+}$ (Fig. 3A,B) and $Irx3^{KO}\ Irx5^{EGFP}/Irx3^{KO}\ Irx5^{EGFP}$ embryos (Fig. 3C,D). Cre-mediated deletion results in complete loss of Irx3 protein 36-48 hours after the onset of Cre activity (R.S. and C.-C.H., unpublished).

Crossing with *Wnt1::Cre* (Brault et al., 2001), which deletes in the neural crest cells that populate the heart and contribute to the development of the OFT, did not result in any structural abnormalities in the heart (Fig. 3E,F). The OFT but not the AV canal defect was recapitulated using *Mef2cAHF::Cre* mice, which express Cre in the myocardial and endocardial cells of anterior heart field derivatives (Verzi et al., 2005), which have been linked to OFT defects, such as DORV (Fig. 3G,H) (Park et al., 2006). To further delineate the specific cell type in which *Irx3* and *Irx5* are required, we used the *Nkx2.5::Cre* transgene to delete these genes in the ventricular myocardium (McFadden et al., 2004; Takeuchi et al., 2011) and *Tie2::Cre* (*Tie2* is also known as *Tek* – Mouse Genome Informatics) to delete in the endocardium (Kisanuki et al., 2001). Whereas the myocardial-specific deletion resulted in no morphological defects (Fig. 3I,J), deletion of *Irx3* and *Irx5* in the endocardium phenocopied the DKO mutant (Fig. 3K,L), with the exception of the DMP defect (Fig. 3L, dashed line). Indeed, the ASD observed using *Tie2::Cre* (Fig. 3L, asterisk) seemed to be due to a defect in the fusion between the AV endocardial cushions and the DMP. In an attempt to understand the cellular origin of the DMP defect and given that the DMP derives from Isl1-expressing second heart field derivatives (Goddeeris et al., 2008), we used *Isl1::Cre* mice, which effectively delete within all second heart field derivatives (Yang et al., 2006). Interestingly, this conditional mutant recapitulated the DKO phenotype, including the lack of DMP, with an additional defect in the tissues targeted in this Cre line in the form of a persistent truncus arteriosus (Fig. 3M, arrowhead), suggesting a genetic interaction between *Irx3*, *Irx5* and *Isl1* (Fig. 3M,N) or that deletion by *Isl1::Cre* in neural crest cells (Engleka et al., 2012) results in an additional phenotype.

Our data demonstrate that the deletion of *Irx3* and *Irx5* in endocardial cells leads to defects in septum formation and OFT alignment, and that there is an additional function for *Irx3* and *Irx5* in the development of DMP.

BMP signaling is misregulated in *Irx3;Irx5* mutant hearts

To identify genes that are misregulated in the *Irx3;Irx5* DKO mutant, we used DNA microarrays to analyze mRNA expression in E12.5 embryonic hearts. At this developmental stage, *Irx3* and *Irx5* are coexpressed in the endocardium lining the AV cushions,

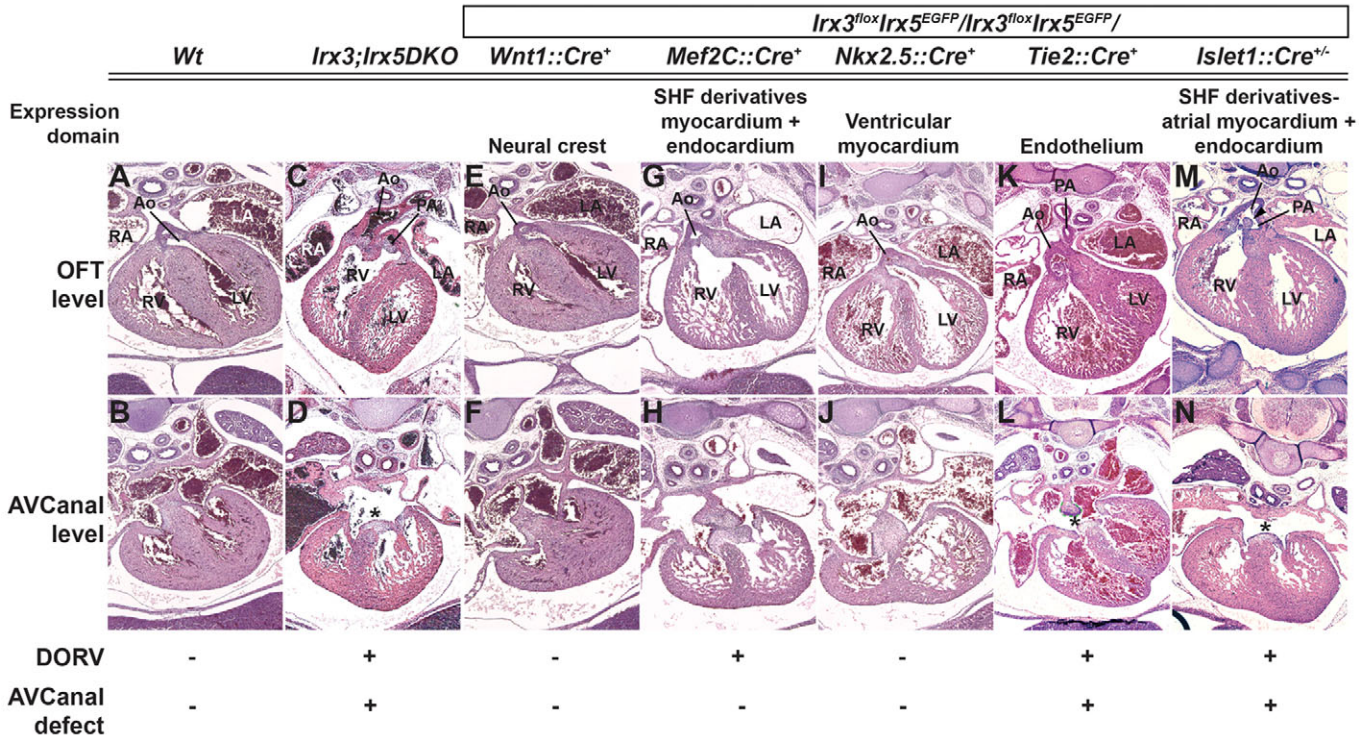

Fig. 3. Determination of the cellular origin of the *Irx3;Irx5* DKO defects in various Cre-expressing mouse lines. Serial H&E-stained sections at the level of the OFT (top row) and AV canal (bottom row). (**A**,**B**) Sections of a wild-type embryo ($Irx3^{+}\ Irx5^{+}/Irx3^{+}\ Irx5^{+}$). (**C**,**D**) Sections of an *Irx3;Irx5* DKO embryo ($Irx3^{KO}\ Irx5^{EGFP}/Irx3^{KO}\ Irx5^{EGFP}$). (**E-N**) Sections of $Irx3^{flox}\ Irx5^{EGFP}/Irx3^{flox}\ Irx5^{EGFP}$ embryos crossed with different Cre-expressing mouse lines, showing that the deletion of *Irx3* and *Irx5* in the endocardium recapitulates the phenotype of the DKO embryos. The expression domain of each Cre line is described above each set of panels. Asterisks indicate an AV canal defect. The presence (+) or absence (–) of DORV and AV canal defect are indicated. RA, right atrium; LA, left atrium; RV, right ventricle; LV, left ventricle; OFT, outflow tract; Ao, aorta; PA, pulmonary artery; SHF, second heart field.

and there are no detectable cardiac abnormalities, such that altered gene expression is therefore likely to reflect early molecular events in altered OFT development. EGFP-positive cells were isolated from dissected hearts using fluorescence-activated cell sorting (FACS) and analyzed for four groups of mice: *Irx3*$^{+}$ *Irx5*^{EGFP}/*Irx3*$^{+}$ *Irx5*$^{+}$ (*Irx5*het), *Irx3*^{KO} *Irx5*^{EGFP}/*Irx3*^{KO} *Irx5*$^{+}$(*Irx3*KO;*Irx5*het), *Irx3*$^{+}$ *Irx5*^{EGFP}/*Irx3*$^{+}$ *Irx5*^{EGFP} (*Irx5*KO) and *Irx3*^{KO} *Irx5*^{EGFP}/*Irx3*^{KO} *Irx5*^{EGFP} (*Irx3;Irx5* DKO) (Fig. 4A). Owing to the need for FACS sorting from the *Irx5*^{EGFP} allele, all genotypes must be at least heterozygous for loss of *Irx5*.

We found 859 genes that were differentially expressed in at least one group versus the wild-type group, with the largest number of misregulated genes in the DKO group. Irx3 and Irx5 act mainly as transcriptional repressors (Costantini et al., 2005; Zhang, S. S. et al., 2011). Accordingly, almost two-thirds of the genes misregulated in DKO hearts are upregulated compared with the *Irx5*het group (Fig. 4B). Unsupervised two-way hierarchal clustering used to group samples based on their gene expression similarities (Fig. 4C) clearly separated DKOs from other samples, showing that they have a distinct transcriptional expression signature. Two discriminatory gene clusters were identified. Cluster A grouped genes downregulated in DKO samples as compared with the other samples and cluster B grouped upregulated genes. Within these two clusters, ten genes are known to be implicated in OFT and vascular defects: *Eln*, *Efnb2*, *Flk1* (*Kdr* – Mouse Genome Informatics), *Flt1*, *Angpt2*, *Slit2*, *Ecscr*, *Adamts9*, *Bmp10* and *Vcan*. Several genes that have been linked to AV canal defects, including *Bmp2*, *Bmp5*, *Bmp10*, *Tgfbr3* and *Runx1t1*, were also significantly changed (Fig. 4C). Misexpression was confirmed by qPCR. *Bmp10* was the most overexpressed (Fig. 4D). Interestingly, several genes linked to the BMP signaling pathway, such as *Sfrp2*, *Tbx20* and *Fosb*, were also misexpressed, consistent with BMP upregulation (Fig. 4E).

Irx3 and Irx5 coordinately regulate *Bmp10* expression

To define the mechanism responsible for misregulation of *Bmp10* in the *Irx3;Irx5* DKO heart, we performed in situ hybridization for

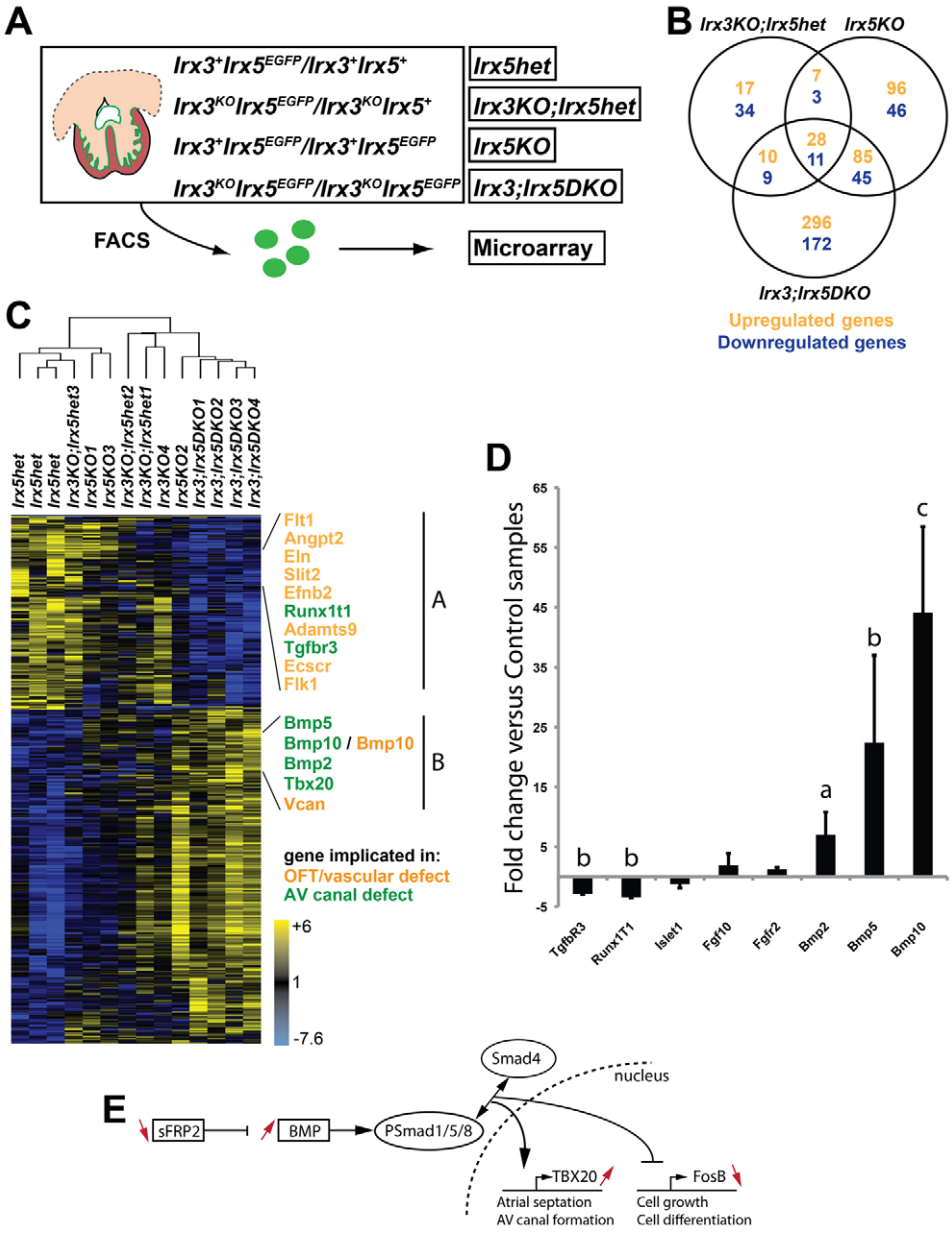

Fig. 4. Dysregulation of cardiac genes in *Irx3* and *Irx5* mutant embryos. (**A**) Genotypes used for microarray. EGFP-positive cells were isolated by FACS. (**B**) Number of genes statistically (P<0.01) upregulated (orange) and downregulated (blue) in each mutant as compared with wild type. (**C**) Unsupervised two-way hierarchal clustering applied to the wild type, *Irx3*KO, *Irx5*KO and *Irx3;Irx5* DKO samples (horizontally) and the 458 statistically differentially expressed genes (vertically). Input consists of replicate expression values for each gene and sample. Gene expression values were centered to the median. Therefore, each color patch represents fold change between expression value and the median, with a continuum from bright blue (lowest) to bright yellow (highest). Two clusters (A and B) containing genes relevant to the discrimination between *Irx3;Irx5* DKO and the other genotypes are shown on the right. (**D**) qPCR confirmation of a number of genes identified by microarray as either downregulated, upregulated or unchanged in the *Irx3;Irx5* DKO. Values are mean ± s.d. a, P<0.05; b, P<0.01; c, P<0.001; in *Irx3;Irx5* DKO versus wild type. (**E**) The BMP pathway and genes described as upstream or downstream components of this pathway. Red arrows illustrate how these genes are misregulated in the *Irx3;Irx5* DKO embryos according to the microarray data.

Bmp10 at E12.5 and E14.5. At E12.5, *Bmp10* was restricted to the ventricular trabecular myocardium, where *Irx3* alone is expressed. Indeed, expression of *Bmp10* was increased in ventricular trabecular myocardium of the *Irx3*KO but not the *Irx5*KO (Fig. 5Aa). In *Irx3;Irx5* DKO hearts, we observed upregulation of *Bmp10* in tissues that express either *Irx3* or *Irx5*, including

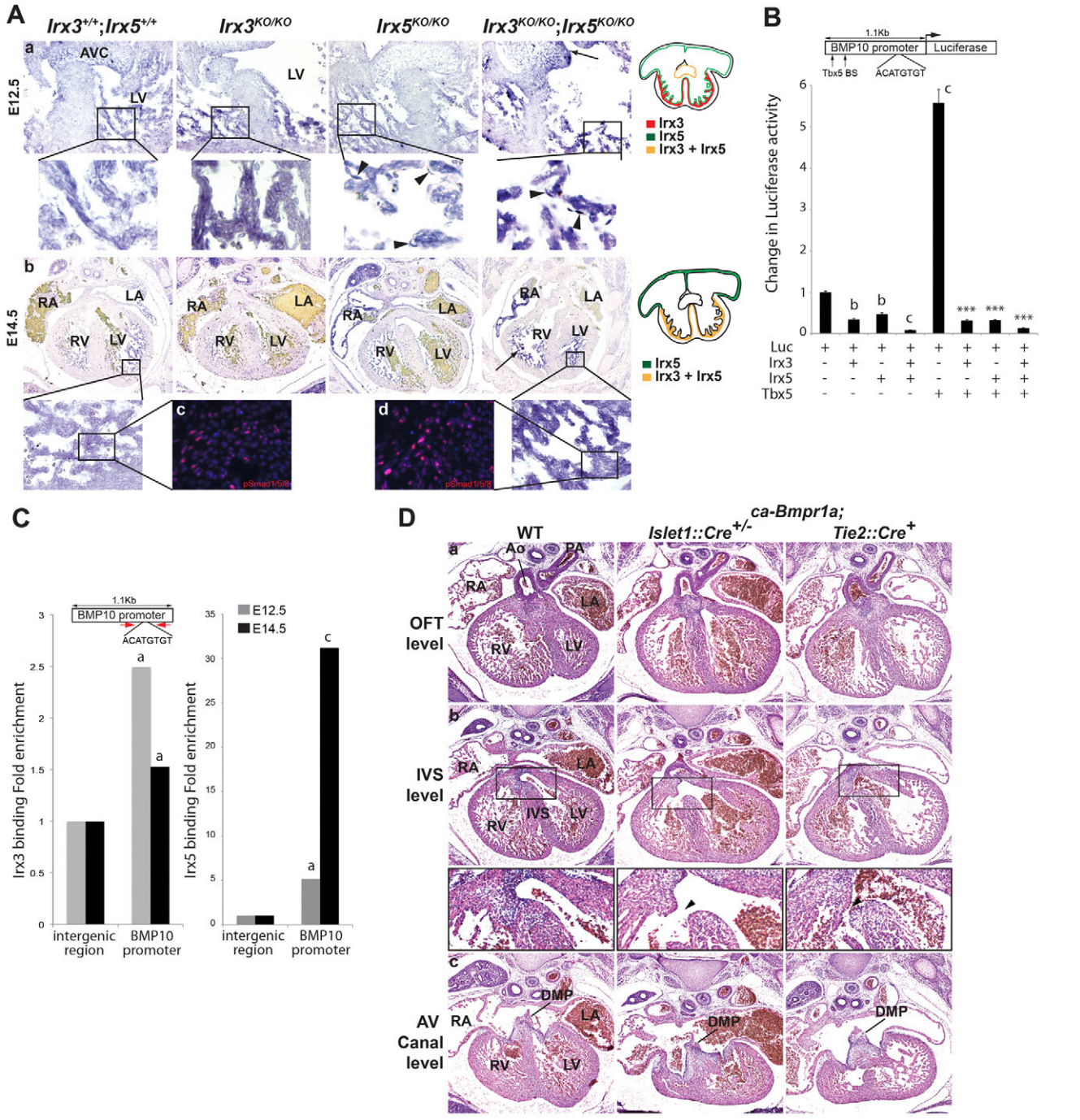

Fig. 5. Regulation of *Bmp10* by Irx3 and Irx5. (**A**) *Bmp10* expression was examined by in situ hybridization on transverse sections of wild-type, *Irx3*KO, *Irx5*KO and *Irx3;Irx5* DKO mouse hearts at E12.5 and E14.5 (Aa,b). Summaries of the expression pattern of *Irx3* and *Irx5* at E12.5 and E14.5 are shown to the right. Immunofluorescence of Smad1/5/8 on wild-type and *Irx3;Irx5* DKO E14.5 hearts (Ac,d). Arrows indicate areas of increased *Bmp10* expression. Arrowheads indicate *Bmp10*-expressing endocardium. (**B**) Change in *Bmp10-luciferase* reporter construct activity by transfection of Irx3 and/or Irx5 and/or Tbx5 expression constructs into Cos7 cells. Values are mean ± s.d. b, $P<0.01$; c, $P<0.001$; versus Luc alone. ***$P<0.001$, versus Tbx5 (ANOVA). Tbx5 BS, Tbx5 binding site. (**C**) SYBR Green PCR amplification (red arrows indicate primers) of an intergenic region and of the Iroquois binding site of the *Bmp10* promoter, after chromatin immunoprecipitation of Irx3 (left) or Irx5 (right) on E12.5 and E14.5 wild-type hearts. a, $P<0.05$; c, $P<0.001$; versus intergenic region (*t*-test). (**D**) Serial sections stained with H&E at the level of the OFT (top row), interventricular septum (middle row) and AV canal (bottom row). Sections of a wild-type embryo and of two *ca-Bmpr1a* embryos crossed with either *Isl1::Cre* or *Tie2::Cre*. Arrowhead indicates ventricular septal defect. RA, right atrium; LA, left atrium; RV, right ventricle; LV, left ventricle; OFT, outflow tract; Ao, aorta; PA, pulmonary artery; IVS, interventricular septum; AV, atrioventricular; DMP, dorsal mesenchymal protrusion.

myocardium and endocardium (arrowheads) of ventricular trabeculae (Fig. 5Aa). We also observed *Bmp10* upregulation in the cardiac domain that coexpresses *Irx3* and *Irx5*, including the endocardium lining the AV cushions, consistent with the observation that the endocardial-specific DKO recapitulates the cardiac phenotype (Fig. 5Aa). At E14.5, *Irx3* and *Irx5* are coexpressed in the ventricular conduction system and trabeculae, and concordantly *Bmp10* expression is increased in these cellular compartments in *Irx3;Irx5* DKO hearts (Fig. 5Ab).

We investigated whether the pathway downstream of *Bmp10* was affected in *Irx3;Irx5* DKO heart. Bmp10 induces Smad1/5/8 phosphorylation (pSmad1/5/8), which leads to Smad translocation to the nucleus to mediate its signaling. By immunofluorescence, we found that the amount and intensity of nuclear pSmad1/5/8 were higher in the DKO ventricular trabeculae, suggesting that Bmp10 activates Smad1/5/8 in the *Irx3;Irx5* DKO hearts (Fig. 5Ac,d).

We then investigated the function of Irx3 and Irx5 in *Bmp10* transcription. We analyzed a 1.1 kb region of the *Bmp10* promoter, located ~1.7 kb upstream of the ATG, that contains a putative consensus Irx binding site (Bilioni et al., 2005). Luciferase analysis showed that Irx3 and Irx5 reduced the baseline activity of this promoter. We also identified two T-box binding sites within the 1.1 kb *Bmp10* promoter. Tbx5 activated the promoter and cotransfection of Irx3 and Irx5 expression constructs prevented this activation. These results show that Irx3 and Irx5 individually or cooperatively repress the expression of *Bmp10* and that they prevent activation of this promoter by Tbx5 (Fig. 5B).

To explore the possibility that Irx repression of *Bmp10* occurs via direct binding, we performed chromatin immunoprecipitation of Irx3 and Irx5 in E12.5 and E14.5 hearts. We tested for enrichment of Irx3 and Irx5 at the putative Irx binding site located in the 1.1 kb promoter region used for the luciferase assay. Irx3 levels at the *Bmp10* promoter were double those at an intergenic region at E12.5 and E14.5 and there was 5-fold and 32-fold more Irx5 in E12.5 and E14.5 hearts, respectively (Fig. 5C). These results show that Irx3 and Irx5 directly bind the *Bmp10* promoter to regulate its expression.

We then further investigated the role of the ectopic endocardial expression of *Bmp10* in the *Irx3;Irx5* DKO phenotype. Knowing that Bmp10 signals through the Bmpr1a receptor (Mazerbourg et al., 2005), we used a genetic manipulation that would be a proxy for increased *Bmp10* expression: we induced cell-specific constitutive activation of Bmpr1a by crossing *ca-Bmpr1a* mice (Kamiya et al., 2008) with *Isl1::Cre* or *Tie2::Cre* mice. At E14.5, the mutant embryos did not display any gross physical abnormalities (data not shown). However, in both cases, expression of *ca-Bmpr1a* led to a membranous VSD similar to that observed in the *Irx3;Irx5* DKO (Fig. 5Db). Conversely, the orientation of the aorta (Fig. 5Da) and the formation of DMP (Fig. 5Dc) appeared normal in these mutants. Together, these data further support the proposal that the endocardial transcriptional repression of *Bmp10* by Irx3 and Irx5 is necessary for proper ventricular septation.

Irx3 and Irx5 are coexpressed in the adult heart

The effect of the combined deletion of *Irx3* and *Irx5* on embryonic heart development clearly indicates overlapping and redundant functions of these two transcription factor genes. As both genes have demonstrated roles in postnatal cardiac physiology, we addressed their roles independent of defective embryonic development. We first analyzed their expression pattern in the adult heart and found that *Irx3* and *Irx5* are coexpressed in the ventricular conduction system, BH and BBs (Fig. 6A-C), as identified by acetylcholinesterase staining (Fig. 6D). The domain of coexpression of Irx3 and Irx5 in the ventricular conduction system extends to the lower nodal cells (LNCs) that connect the AV node to the BH (Fig. 6E-H) (Aanhaanen et al., 2009). This suggests a shared role for *Irx3* and *Irx5* in the function of the conduction system. Within the ventricular septum, *Irx3* and *Irx5* were expressed in a gradient, specifically in myocardial cells, as shown by their coexpression with tropomyosin (Fig. 6I-L). This gradient of expression was found in the myocardium of the right and left ventricular walls, with highest expression in the endocardial region (Fig. 6M-T).

Coexpression of Irx3 and Irx5 is necessary for cardiac function

To address the combinatorial roles of *Irx3* and *Irx5* in the adult heart, we bypassed the embryonic lethality and cardiac structural defects by inducing the deletion of *Irx3* in the postnatal heart with concomitant loss of *Irx5* function. We used the *Myh6-Cre/Esr1* mouse strain, which expresses the Cre-estrogen receptor fusion protein under control of the cardiac myocyte-specific *Myh6* promoter (Sohal et al., 2001), and activated the Cre with five consecutive tamoxifen injections. We confirmed that our protocol reduced the number of *Irx3* transcripts (Fig. 7A). Telemetry electrocardiogram analysis of 9-week-old WT (*Irx3*$^{+}$ *Irx5*$^{+}$*/Irx3*$^{+}$ *Irx5*$^{+}$*/Myh6::Cre*$^{+}$), *Irx3*KO, *Irx5*KO and *Irx3;Irx5* DKO mice showed a prolonged QRS and an RR′ shape in the *Irx3;Irx5* DKO mice, similar to the *Irx3*KO mice (Fig. 7B,C, black arrow), suggesting that this phenotype is due to the lack of *Irx3* only. Intriguingly, the loss of the T wave normally observed in *Irx5*KO mice was restored to normal in the inducible DKO (Fig. 7B, red arrow), suggesting a counterbalance of *Irx3* and *Irx5* function in regulating the ventricular repolarization. The DKO mice were uniquely characterized by a prolonged PR interval, reflecting a conduction delay through the proximal part of the ventricular conduction system, at the level of the AV node, BH and/or BBs (Fig. 7C). No spontaneous arrhythmias were observed in any of the genotypes throughout the telemetry traces (data not shown). These results clearly show a postnatal genetic interaction between *Irx3* and *Irx5*.

Cardiac electrophysiological activity is a reflection of the combined function of multiple ion channels and gap junctions. Thus, failure in their normal activity leads to changes in the ECG waveforms and ultimately to various types of inherited arrhythmia syndromes. We analyzed the expression pattern of several ion channel and gap junction proteins that sculpt the ECG features affected in the DKO mice. The prolongation of the QRS in the *Irx3*KO mice is associated with reduced Cx40 (Gja5 – Mouse Genome Informatics) expression in the VCS (Zhang, S. S. et al., 2011). Whereas its expression was unaltered in *Irx5*KO hearts, Cx40 levels were markedly reduced in the BH of the *Irx3*KO and *Irx3;Irx5* DKO mice (Fig. 7D). This result supports our hypothesis that the QRS prolongation in the DKO mice is due to the deletion of *Irx3* only. Reduction in the levels of the sodium channel protein Nav1.5 have been implicated in PR prolongation (Papadatos et al., 2002; Smits et al., 2002; Royer et al., 2005; Pfeufer et al., 2010), and we found that its expression was much reduced in the BH in DKO mice compared with the other genotypes (Fig. 7E). Therefore, Irx3 and Irx5 have individual roles in some aspects of the conduction system, as well as redundant functions in regulating Nav1.5 expression.

Restoration of the repolarization wave in the ECG of the DKOs indicated a more complicated relationship between Irx3 and Irx5.

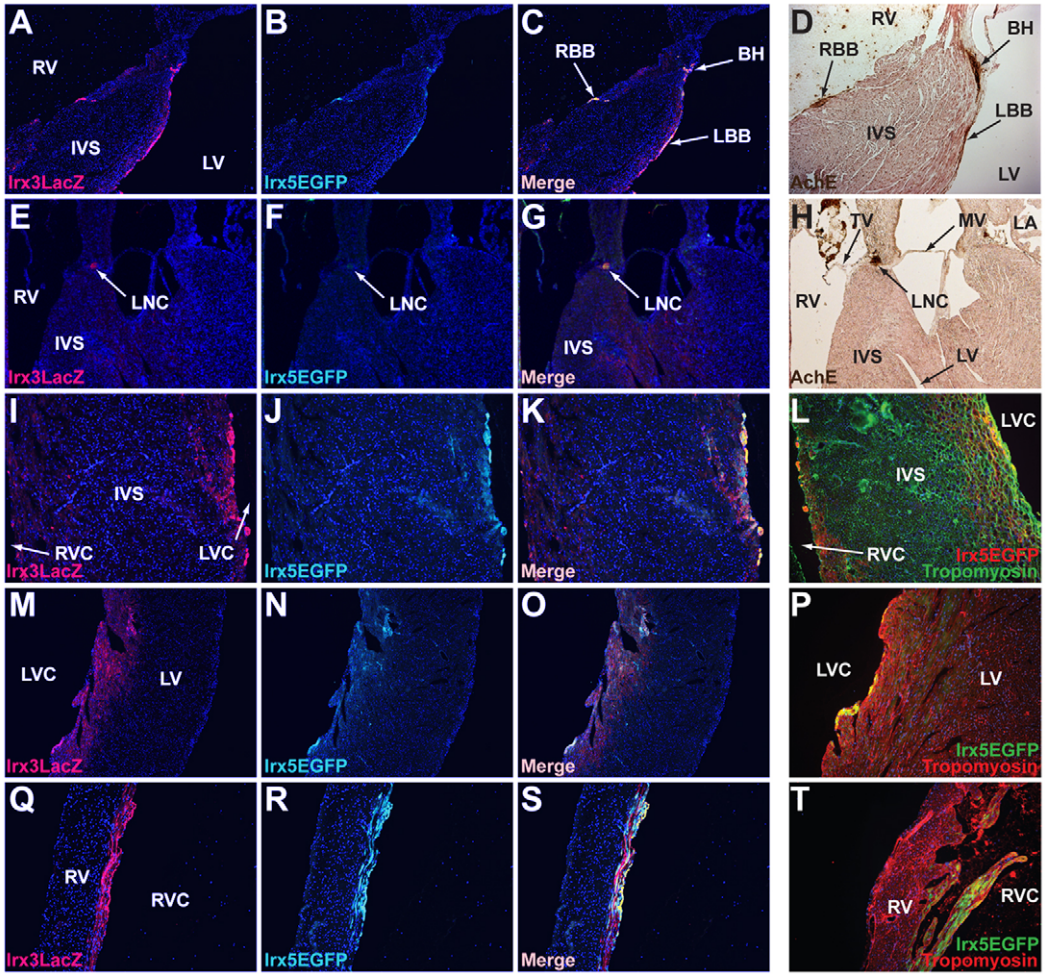

Fig. 6. Expression of *Irx3* and *Irx5* in the adult heart. (**A-C**) Immunofluorescence colocalization of $Irx3^{taulacZ}$ (red) and $Irx5^{EGFP}$ (green) in the ventricular conduction system of $Irx3^{taulacZ/+};Irx5^{EGFP/+}$ adult mouse heart. (**E-G**) Coexpression of Irx3 and Irx5 in the lower nodal cells (LNCs) that connect the AV node to the BH. (**D**,**H**) Acetylcholinesterase staining (brown) of serial sections marks the conducting cells and confirms the expression of *Irx3* and *Irx5* in the ventricular conduction system. (**I-L**) In the interventricular septum, *Irx3* and *Irx5* are expressed in a gradient and colocalize with tropomyosin (L). (**M-T**) Immunofluorescence at the level of the left ventricular wall (M-P) and the right ventricular wall (Q-T) showing a gradient of expression of *Irx3* and *Irx5*, with higher expression in the endocardial region that colocalizes with tropomyosin. BH, bundle of his; RBB, right bundle branch; LBB, left bundle branch; RV, right ventricle; LV, left ventricle; IVS, interventricular septum; MV, mitral valves; TV, tricuspid valves; RVC, right ventricular chamber; LVC, left ventricular chamber.

This was borne out by molecular analysis of components of the repolarization gradient. As reported, loss of the T wave in the *Irx5*KO was associated with the loss of gradient in the potassium channel Kv4.2 (Kcnd2 – Mouse Genome Informatics) within the ventricular wall. We found that this gradient was maintained in the *Irx3*KO and was recovered in *Irx3;Irx5* DKO mice, in which the T wave is present (Fig. 7F). This indicates that Irx5 normally prevents Irx3 from activating the expression of Kv4.2 and that, in the absence of both Irx factors, the normal pattern of Kv4.2 expression is maintained, suggesting the existence of additional activating or repressing factors that control the repolarization gradient.

DISCUSSION

We showed essential redundant roles of *Irx3* and *Irx5* in the developing mouse heart. Their overlapping expression and functional redundancy in the endocardium ensure completion of atrial and ventricular septation and proper positioning of the great arteries. In addition, our data show that continued expression of *Irx3* and *Irx5* in adult cardiomyocytes is necessary for proper cardiac electrophysiological activity. Thus, we found two temporal-specific roles for *Irx3* and *Irx5* in the heart: control of embryonic morphogenesis and regulation of adult heart function.

Functional redundancy of mammalian Irx transcription factors during embryogenesis

We demonstrated genetic redundancy of Irx factors, as the combined deletion of *Irx3* and *Irx5* leads to striking structural heart defects not observed in the *Irx3* or *Irx5* singly deficient mice. Recapitulation of the abnormal septation phenotype with the endothelial-specific *Tie2::Cre* strongly suggests functional significance for both *Irx3* and *Irx5* in the endothelial cell lineage. This indicates a sensitive subset of cardiac cells within which the redundancy between *Irx3* and *Irx5* is most apparent, and suggests that other Irx genes expressed in myocardium might compensate for their combined loss in the myocardium.

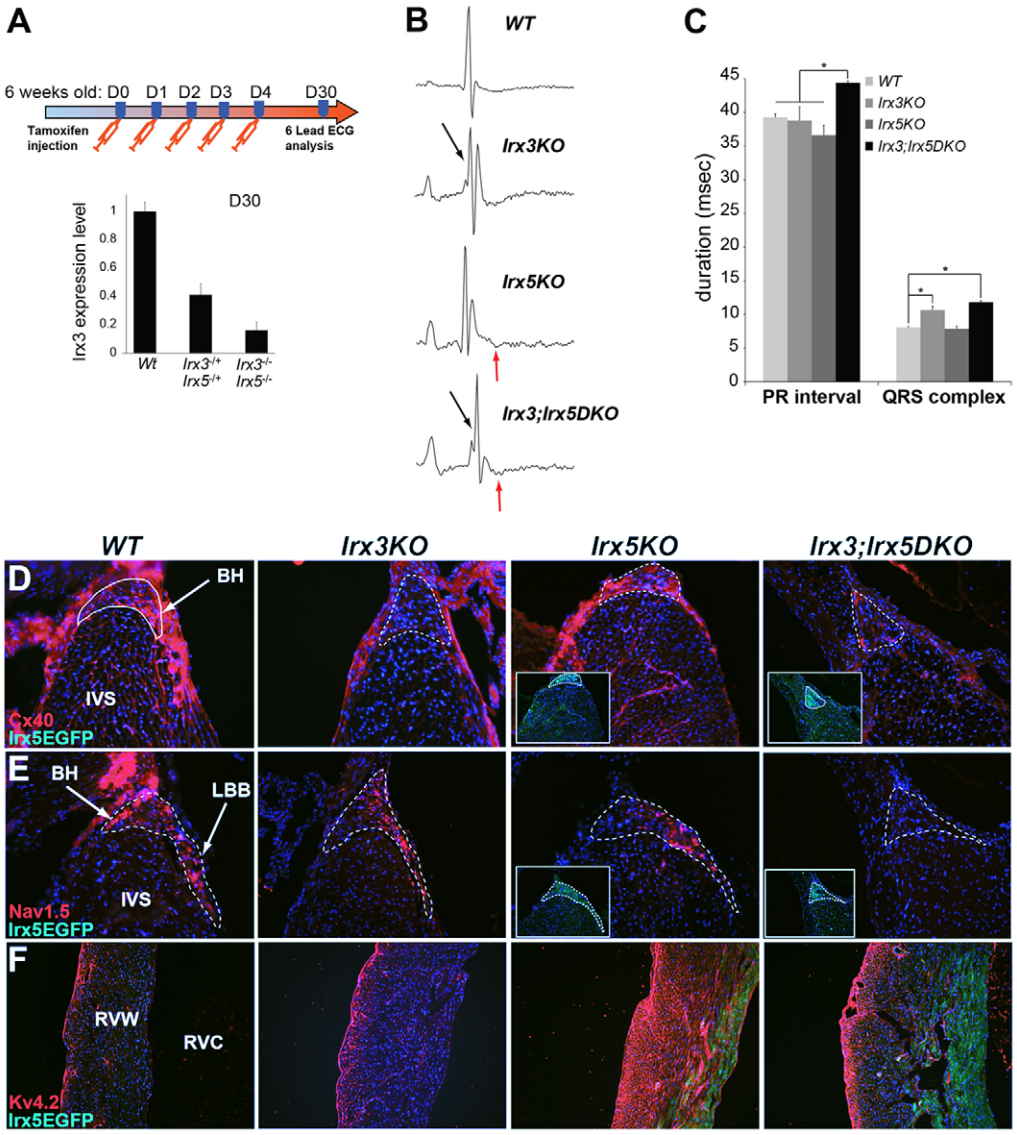

Fig. 7. Electrophysiological analysis of *Irx3* and *Irx5* mutant adult mice. (**A**) Protocol of tamoxifen injection of *Irx3*^{flox} *Irx5*^{EGFP}/*Irx3*^{flox} *Irx5*^{EGFP}/*Myh6::MerCreMer* 6-week-old mice. Two weeks after injections for five consecutive days, electrocardiograms are recorded using six leads and telemetry. qPCR analysis shows successful reduction of *Irx3* expression in *Irx3*^{flox} *Irx5*^{EGFP}/*Irx3*$^{+}$ *Irx5*$^{+}$/*Myh6::MerCreMer* and *Irx3*^{flox} *Irx5*^{EGFP}/*Irx3*^{flox} *Irx5*^{EGFP}/*Myh6::MerCreMer* hearts. Values are fold WT level, mean ± s.e.m. (**B**) Representative six-lead ECG analysis from WT (*Irx3*$^{+}$ *Irx5*$^{+}$/*Irx3*$^{+}$ *Irx5*$^{+}$/*Myh6::Cre*$^{+}$), *Irx3*KO (*Irx3*$^{taulacZ/taulacZ}$), *Irx5*KO (*Irx3*^{flox} *Irx5*^{EGFP}/*Irx3*^{flox} *Irx5*^{EGFP}/*Myh6::Cre*$^{-}$) and *Irx3;Irx5* DKO (*Irx3*^{flox} *Irx5*^{EGFP}/*Irx3*^{flox} *Irx5*^{EGFP}/*Myh6::Cre*$^{+}$) showing prolongation and RR′ shape of the QRS in both *Irx3*KO and *Irx5*KO (black arrow), recovery of the T wave in *Irx3;Irx5* DKO as compared with *Irx5*KO (red arrow), and prolongation of the PR interval in *Irx3;Irx5* DKO mice as compared with the other genotypes. (**C**) PR interval and QRS complex measurements in the four genotypes. Values are mean ± s.e.m.; *n*=4-6; **P*<0.05. (**D-F**) Immunofluorescence of (D) Cx40 and (E) Nav1.5 (red) at the level of the ventricular conduction system, as confirmed by the EGFP staining of the BH and BBs (green), and (F) Kv4.2 (red) at the level of the right ventricular wall, with EGFP staining showing the endocardium-to-epicardium gradient of Irx5 expression (green). IVS, interventricular septum; RVW, right ventricular wall; RVC, right ventricular chamber; LBB, left bundle branch.

The *Irx3;Irx5* DKO mice also have a DMP defect. DMP derives from *Isl1*-expressing progenitors but is not endothelial-derived (Mommersteeg et al., 2006), suggesting that the DMP deficiency is not directly due to the *Irx3* and *Irx5* deficiency in the AV cushion endocardium. As expected, the DMP is present when endocardial Irx3 expression is removed using *Tie2::Cre*, but it fails to fuse to the AV cushions, leading to an ASD. Conversely, the use of *Isl1::Cre* recapitulates the absence of the DMP.

Dysregulation of a broad transcriptional program in the DKOs further demonstrates the functional redundancy between *Irx3* and *Irx5*. Among these genes, we identified several that are implicated in OFT and AV canal formation, including members of the BMP family, which are upregulated in the *Irx3;Irx5* DKO hearts. These growth factors have crucial roles in the embryonic development of several organs, including the heart: their overexpression, deletion or mutation leads to various cardiac defects (Evans et al., 2010). A link between Iroquois genes and BMPs was reported in *Xenopus*, in which the ortholog of mouse *Irx1* inhibits *Bmp4* expression during neural differentiation (Gomez-Skarmeta et al., 2001).

Here we show that, in the mammalian heart, Irx3 and/or Irx5 directly inhibits the expression of *Bmp10*. In the *Irx3;Irx5* DKO E12.5 hearts, *Bmp10* is misexpressed in the endocardial cells that line the ventricular trabeculae and the endocardial cushions. The ectopic expression of *Bmp10* in the endocardium supports our model of redundancy between *Irx3* and *Irx5* in repressing expression of this gene. By E14.5, however, *Bmp10* returns to its myocardial-specific pattern, consistent with the restricted expression of *Irx3* and *Irx5* to myocardium at this stage. *Bmp10* regulates cardiac morphogenesis. *Bmp10*-deficient mice do not survive past E10.5 due to a range of cardiovascular defects, including abnormal OFT and AV endocardial cushion development (Chen et al., 2004). Myocardial-specific Bmp10 overexpression leads to normal embryonic development but abnormal postnatal cardiomyocyte hypertrophic growth and subaortic narrowing (Chen et al., 2006). As proxy for the overexpression of Bmp10, we tested the effect of activating BMP signaling in the endocardium, and found a defect in cardiac ventricular septation, suggesting that ectopic endocardial expression of *Bmp10* in the *Irx3;Irx5* DKO contributes to the phenotype. This effect is specific, as we found that activation of BMP signaling within a tissue that is not known to be directly dependent on BMP signaling (in the DMP using *Isl1::Cre*) does not lead to defects in its formation.

The T-box transcription factor *Tbx20* is a direct target of the Bmp10/Smad1 signaling pathway, and is upregulated in the myocardium of *αMHC-BMP10* transgenic mice (Mandel et al., 2010; Zhang, W. et al., 2011). During embryonic development, *Tbx20* is strongly expressed in the atria and the endocardium lining the AV cushions and exhibits more modest expression in the ventricular myocardium (Zhang, W. et al., 2011). A *TBX20* gain-of-function mutation in human causes AV canal defects including ASD (Posch et al., 2010), and *TBX20* is upregulated in patients with tetralogy of Fallot (Hammer et al., 2008). We observed an increase in nuclear staining of Smad1/5/8 in *Irx3;Irx5* DKO hearts and upregulation of *Tbx20* in the endocardial sorted cells of the *Irx3;Irx5* DKO hearts as compared with control hearts. This suggests that, during cardiac development, *Irx3* and *Irx5* might participate in a BMP-dependent pathway that represses *Tbx20* expression in the endocardium, ensuring proper OFT and AV canal formation.

Redundant and unique regulation of adult electrophysiological activity by Irx genes

Irx3 and *Irx5* singly deficient mice are characterized by specific defects in adult electrophysiological activity of the heart, suggesting that, unlike their role in embryonic heart morphogenesis, these transcription factors are not fully redundant in the regulation of postnatal electrical activity. The deletion of *Irx3* slows and disorganizes the ventricular conduction of the electrical influx through reduction of Cx40 and ectopic expression of Cx43 (Gja1 – Mouse Genome Informatics) in the proximal BBs (Zhang, S. S. et al., 2011). *Irx5*-deficient mice exhibit abnormal cardiac ventricular repolarization due to a defect in the establishment of the epicardium-to-endocardium gradient of the ion channel Kv4.2 and its current $I_{to,f}$ (Costantini et al., 2005).

Bypassing the embryonic cardiac structural heart defects, we created a postnatal *Irx3*- and *Irx5*-deficient mouse and observed several electrophysiological defects. The prolongation of the QRS complex was found in both *Irx3*KO and *Irx3;Irx5* DKO hearts, and, accordingly, expression of Cx40 was reduced in the BH in these two genotypes. This suggests that the prolongation of the QRS is due specifically to the lack of *Irx3* and that *Irx5* does not significantly contribute to regulation of Cx40 expression. One characteristic of the DKO ECG that has not been observed in the single KOs is the prolongation of the PR interval, and, together with this result, we found a DKO-specific reduction in expression in the sodium channel Nav1.5 in the BH. This PR prolongation might be due to a delay in conduction through the atria, the AV node and/or the BH. Increase in duration of the PR interval has been described previously in mice heterozygous for a deletion of the *Nav1.5* (*Scn5a*) gene (Papadatos et al., 2002; Royer et al., 2005). Furthermore, Brugada syndrome patients carrying a loss-of-function mutation in *SCN5A* have a prolonged PR interval associated with a delay in BH to ventricular conduction (Smits et al., 2002). In the adult, *Irx3* and *Irx5* are coexpressed in the ventricular conduction system, including LNCs and BH, but are not expressed in the AV node, suggesting that the PR prolongation is due to the downregulation of *Scn5a* in the BH domain. The additional reduction of expression of Cx40 might also contribute to this phenotype.

Surprisingly, the lack of a T wave in the *Irx5*-deficient mice was not observed in *Irx3;Irx5* DKO mice, suggesting a rescue of the cardiac repolarization gradient. We analyzed the expression pattern of Kv4.2, which underlies the $I_{to,f}$ current essential for the formation of the T wave. Whereas its ventricular gradient of expression was lost in the *Irx5*KO mice, it was present in *Irx3*KO mice and recovered in the *Irx3;Irx5* DKO mice. This suggests antagonistic effects between Irx3 and Irx5 in the regulation of this ion channel. Consistent with this notion, an in vitro study in the rat showed that Iroquois genes have antagonistic effects in the regulation of the *Kv4.2* gene, as Irx4 suppresses the effect of Irx5 on its promoter (He et al., 2009). The present expression analysis suggests that, in the subendocardial myocardium, Kv4.2 expression is regulated by several factors, with different levels of control. Concordant with previous reports, in wild-type and *Irx3*KO mice, the dominant regulator, Irx5, inhibits Kv4.2 expression to create the gradient (Costantini et al., 2005). A possible explanation for this phenotype is that, in the *Irx5*KO mice, Irx3 is the transcriptional regulator that is likely to take over, upregulating this ion channel in the subendocardial myocardium, abolishing its expression gradient.

When both Irx3 and Irx5 are absent, we propose that another, as yet unidentified, factor with a similar endocardium-to-epicardium gradient of activity inhibits the expression of Kv4.2, recreating its gradient. In pathological situations, other transcription factors regulate the expression of Kv4 ion channels, such as Gata4- and Gata6-Fog2 (Zfpm2) and Calcineurin/NFATc3 (Jia and Takimoto, 2003; Rossow et al., 2004). It will be interesting to investigate whether one of these pathways inhibits Kv4.2 expression and recreates its gradient of expression in the absence of Irx5 and Irx3.

Summary

We have shown that *Irx3* and *Irx5* function redundantly in heart development and both redundantly and antagonistically in regulating postnatal cardiac electrophysiology. Recessive *IRX5* mutations result in cardiac structural and electrophysiological defects as part of Hamamy syndrome (Bonnard et al., 2012). It is not clear whether the human *IRX5* mutations lead to simple loss of IRX5 function or whether they cause a broader dominant effect, but the disparity between mutations in *IRX5* and the mouse *Irx5* loss of function might also be explained by differences in the function of Irx5 in mouse and human. Nonetheless, the similarities in phenotype between the *Irx3;Irx5* DKO mice described here and the cardiac features of Hamamy

syndrome provide a direct link to human disease and might lead to new insights into the as yet poorly understood etiology of congenital heart defects (Bruneau, 2008).

Acknowledgements
We thank Linda Ta (Gladstone Genomics Core), Alex Williams (Gladstone Bioinformatics Core) and Caroline Miller (Gladstone Histology Core) for technical support and G. Howard for editorial assistance.

Funding
N.G. was funded by American Heart Association fellowships. This work was funded by grants from the Canadian Institutes of Health Research (C.-C.H.), the National Institutes of Health (NIH) National Heart, Lung, and Blood Institute (NHLBI) [R01 HL93414 ARRA to B.G.B.]; and the Lawrence J. and Florence A. DeGeorge Charitable Trust/American Heart Association Established Investigator Award [to B.G.B.]. This work was also supported by an NIH National Center for Research Resources (NCRR) grant [C06 RR018928] to the J. David Gladstone Institutes and by William H. Younger, Jr [B.G.B.]. Deposited in PMC for release after 12 months.

Competing interests statement
The authors declare no competing financial interests.

References

Aanhaanen, W. T., Brons, J. F., Dominguez, J. N., Rana, M. S., Norden, J., Airik, R., Wakker, V., de Gier-de Vries, C., Brown, N. A., Kispert, A. et al. (2009). The Tbx2+ primary myocardium of the atrioventricular canal forms the atrioventricular node and the base of the left ventricle. *Circ. Res.* **104**, 1267-1274.

Benjamini, Y. and Hochberg, Y. (1995). Controlling the false discovery rate: a practical and powerful approach to multiple testing. *J. Royal Stat. Soc. Series B* **57**, 289-300.

Bilioni, A., Craig, G., Hill, C. and McNeill, H. (2005). Iroquois transcription factors recognize a unique motif to mediate transcriptional repression in vivo. *Proc. Natl. Acad. Sci. USA* **102**, 14671-14676.

Bonnard, C., Strobl, A. C., Shboul, M., Lee, H., Merriman, B., Nelson, S. F., Ababneh, O. H., Uz, E., Guran, T., Kayserili, H. et al. (2012). Mutations in IRX5 impair craniofacial development and germ cell migration via SDF1. *Nat. Genet.* **44**, 709-713.

Brault, V., Moore, R., Kutsch, S., Ishibashi, M., Rowitch, D. H., McMahon, A. P., Sommer, L., Boussadia, O. and Kemler, R. (2001). Inactivation of the beta-catenin gene by Wnt1-Cre-mediated deletion results in dramatic brain malformation and failure of craniofacial development. *Development* **128**, 1253-1264.

Bruneau, B. G. (2008). The developmental genetics of congenital heart disease. *Nature* **451**, 943-948.

Bruneau, B. G., Bao, Z. Z., Fatkin, D., Xavier-Neto, J., Georgakopoulos, D., Maguire, C. T., Berul, C. I., Kass, D. A., Kuroski-de Bold, M. L., de Bold, A. J. et al. (2001). Cardiomyopathy in Irx4-deficient mice is preceded by abnormal ventricular gene expression. *Mol. Cell. Biol.* **21**, 1730-1736.

Burglin, T. R. (1997). Analysis of TALE superclass homeobox genes (MEIS, PBC, KNOX, Iroquois, TGIF) reveals a novel domain conserved between plants and animals. *Nucleic Acids Res.* **25**, 4173-4180.

Cavodeassi, F., Modolell, J. and Gomez-Skarmeta, J. L. (2001). The Iroquois family of genes: from body building to neural patterning. *Development* **128**, 2847-2855.

Chen, H., Shi, S., Acosta, L., Li, W., Lu, J., Bao, S., Chen, Z., Yang, Z., Schneider, M. D., Chien, K. R. et al. (2004). BMP10 is essential for maintaining cardiac growth during murine cardiogenesis. *Development* **131**, 2219-2231.

Chen, H., Yong, W., Ren, S., Shen, W., He, Y., Cox, K. A., Zhu, W., Li, W., Soonpaa, M., Payne, R. M. et al. (2006). Overexpression of bone morphogenetic protein 10 in myocardium disrupts cardiac postnatal hypertrophic growth. *J. Biol. Chem.* **281**, 27481-27491.

Christoffels, V. M., Keijser, A. G., Houweling, A. C., Clout, D. E. and Moorman, A. F. (2000). Patterning the embryonic heart: identification of five mouse Iroquois homeobox genes in the developing heart. *Dev. Biol.* **224**, 263-274.

Costantini, D., Arruda, E. P., Agarwal, P., Kim, K.-H., Zhu, Y., Zhu, W., Lebel, M., Cheng, C., Park, C. Y., Pierce, S. A. et al. (2005). The homeodomain transcription factor Irx5 establishes the mouse cardiac ventricular repolarization gradient. *Cell* **123**, 347-358.

Eisen, M. B., Spellman, P. T., Brown, P. O. and Botstein, D. (1998). Cluster analysis and display of genome-wide expression patterns. *Proc. Natl. Acad. Sci. USA* **95**, 14863-14868.

Engleka, K. A., Manderfield, L. J., Brust, R. D., Li, L., Cohen, A., Dymecki, S. M. and Epstein, J. A. (2012). Islet1 derivatives in the heart are of both neural crest and second heart field origin. *Circ. Res.* **110**, 922-926.

Evans, S. M., Yelon, D., Conlon, F. L. and Kirby, M. L. (2010). Myocardial lineage development. *Circ. Res.* **107**, 1428-1444.

Goddeeris, M. M., Rho, S., Petiet, A., Davenport, C. L., Johnson, G. A., Meyers, E. N. and Klingensmith, J. (2008). Intracardiac septation requires hedgehog-dependent cellular contributions from outside the heart. *Development* **135**, 1887-1895.

Gomez-Skarmeta, J., de La Calle-Mustienes, E. and Modolell, J. (2001). The Wnt-activated Xiro1 gene encodes a repressor that is essential for neural development and downregulates Bmp4. *Development* **128**, 551-560.

Gomez-Skarmeta, J. L., del Corral, R. D., de la Calle-Mustienes, E., Ferre-Marco, D. and Modolell, J. (1996). *Araucan* and *caupolican*, two members of the novel *iroquois* complex, encode homeoproteins that control proneural and vein-forming genes. *Cell* **85**, 95-105.

Hammer, S., Toenjes, M., Lange, M., Fischer, J. J., Dunkel, I., Mebus, S., Grimm, C. H., Hetzer, R., Berger, F. and Sperling, S. (2008). Characterization of TBX20 in human hearts and its regulation by TFAP2. *J. Biol. Chem.* **104**, 1022-1033.

He, W., Jia, Y. and Takimoto, K. (2009). Interaction between transcription factors Iroquois proteins 4 and 5 controls cardiac potassium channel Kv4.2 gene transcription. *Cardiovasc. Res.* **81**, 64-71.

Houweling, A. C., Dildrop, R., Peters, T., Mummenhoff, J., Moorman, A. F., Ruther, U. and Christoffels, V. M. (2001). Gene and cluster-specific expression of the Iroquois family members during mouse development. *Mech. Dev.* **107**, 169-174.

Itoh, M., Kudoh, T., Dedekian, M., Kim, C. H. and Chitnis, A. B. (2002). A role for iro1 and iro7 in the establishment of an anteroposterior compartment of the ectoderm adjacent to the midbrain-hindbrain boundary. *Development* **129**, 2317-2327.

Jia, Y. and Takimoto, K. (2003). GATA and FOG2 transcription factors differentially regulate the promoter for Kv4.2 K(+) channel gene in cardiac myocytes and PC12 cells. *Cardiovasc. Res.* **60**, 278-287.

Kamiya, N., Ye, L., Kobayashi, T., Mochida, Y., Yamauchi, M., Kronenberg, H. M., Feng, J. Q. and Mishina, Y. (2008). BMP signaling negatively regulates bone mass through sclerostin by inhibiting the canonical Wnt pathway. *Development* **135**, 3801-3811.

Kisanuki, Y. Y., Hammer, R. E., Miyazaki, J., Williams, S. C., Richardson, J. A. and Yanagisawa, M. (2001). Tie2-Cre transgenic mice: a new model for endothelial cell-lineage analysis in vivo. *Dev. Biol.* **230**, 230-242.

Lickert, H., Takeuchi, J. K., von Both, I., Walls, J. R., McAuliffe, F., Adamson, S. L., Henkelman, R. M., Wrana, J. L., Rossant, J. and Bruneau, B. G. (2004). Baf60c is essential for function of BAF chromatin remodelling complexes in heart development. *Nature* **432**, 107-112.

Mandel, E. M., Kaltenbrun, E., Callis, T. E., Zeng, X. X., Marques, S. R., Yelon, D., Wang, D. Z. and Conlon, F. L. (2010). The BMP pathway acts to directly regulate Tbx20 in the developing heart. *Development* **137**, 1919-1929.

Mazerbourg, S., Sangkuhl, K., Luo, C. W., Sudo, S., Klein, C. and Hsueh, A. J. (2005). Identification of receptors and signaling pathways for orphan bone morphogenetic protein/growth differentiation factor ligands based on genomic analyses. *J. Biol. Chem.* **280**, 32122-32132.

McFadden, D. G., Barbosa, A. C., Richardson, J. A., Schneider, M. D., Srivastava, D. and Olson, E. N. (2004). The Hand1 and Hand2 transcription factors regulate expansion of the embryonic cardiac ventricles in a gene dosage-dependent manner. *Development* **132**, 189-201.

Mommersteeg, M. T., Soufan, A. T., de Lange, F. J., van den Hoff, M. J., Anderson, R. H., Christoffels, V. M. and Moorman, A. F. (2006). Two distinct pools of mesenchyme contribute to the development of the atrial septum. *Circ. Res.* **99**, 351-353.

Mummenhoff, J., Houweling, A. C., Peters, T., Christoffels, V. M. and Ruther, U. (2001). Expression of Irx6 during mouse morphogenesis. *Mech. Dev.* **103**, 193-195.

Olson, E. N. (2006). Gene regulatory networks in the evolution and development of the heart. *Science* **313**, 1922-1927.

Papadatos, G. A., Wallerstein, P. M., Head, C. E., Ratcliff, R., Brady, P. A., Benndorf, K., Saumarez, R. C., Trezise, A. E., Huang, C. L., Vandenberg, J. I. et al. (2002). Slowed conduction and ventricular tachycardia after targeted disruption of the cardiac sodium channel gene Scn5a. *Proc. Natl. Acad. Sci. USA* **99**, 6210-6215.

Park, E. J., Ogden, L. A., Talbot, A., Evans, S., Cai, C. L., Black, B. L., Frank, D. U. and Moon, A. M. (2006). Required, tissue-specific roles for Fgf8 in outflow tract formation and remodeling. *Development* **133**, 2419-2433.

Peters, T., Ausmeier, K., Dildrop, R. and Ruther, U. (2002). The mouse Fused toes (Ft) mutation is the result of a 1.6-Mb deletion including the entire Iroquois B gene cluster. *Mamm. Genome* **13**, 186-188.

Pfeufer, A., van Noord, C., Marciante, K. D., Arking, D. E., Larson, M. G., Smith, A. V., Tarasov, K. V., Muller, M., Sotoodehnia, N., Sinner, M. F. et al. (2010). Genome-wide association study of PR interval. *Nat. Genet.* **42**, 153-159.

Posch, M. G., Gramlich, M., Sunde, M., Schmitt, K. R., Lee, S. H., Richter, S., Kersten, A., Perrot, A., Panek, A. N., Al Khatib, I. H. et al. (2010). A gain-of-function TBX20 mutation causes congenital atrial septal defects, patent foramen ovale and cardiac valve defects. *J. Med. Genet.* **47**, 230-235.

Rossow, C. F., Minami, E., Chase, E. G., Murry, C. E. and Santana, L. F. (2004). NFATc3-induced reductions in voltage-gated K^+ currents after myocardial infarction. *Circ. Res.* **94**, 1340-1350.

Royer, A., van Veen, T. A., Le Bouter, S., Marionneau, C., Griol-Charhbili, V., Leoni, A. L., Steenman, M., van Rijen, H. V., Demolombe, S., Goddard, C. A. et al. (2005). Mouse model of SCN5A-linked hereditary Lenegre's disease: age-related conduction slowing and myocardial fibrosis. *Circulation* **111**, 1738-1746.

Sharpe, J., Ahlgren, U., Perry, P., Hill, B., Ross, A., Hecksher-Sorensen, J., Baldock, R. and Davidson, D. (2002). Optical projection tomography as a tool for 3D microscopy and gene expression studies. *Science* **296**, 541-545.

Smits, J. P., Eckardt, L., Probst, V., Bezzina, C. R., Schott, J. J., Remme, C. A., Haverkamp, W., Breithardt, G., Escande, D., Schulze-Bahr, E. et al. (2002). Genotype-phenotype relationship in Brugada syndrome: electrocardiographic features differentiate SCN5A-related patients from non-SCN5A-related patients. *J. Am. Coll. Cardiol.* **40**, 350-356.

Sohal, D. S., Nghiem, M., Crackower, M. A., Witt, S. A., Kimball, T. R., Tymitz, K. M., Penninger, J. M. and Molkentin, J. D. (2001). Temporally regulated and tissue-specific gene manipulations in the adult and embryonic heart using a tamoxifen-inducible cre protein. *Circ. Res.* **89**, 20-25.

Srivastava, D. (2006). Making or breaking the heart: from lineage determination to morphogenesis. *Cell* **126**, 1037-1048.

Takeuchi, J. K., Lou, X., Alexander, J. M., Sugizaki, H., Delgado-Olguin, P., Holloway, A. K., Mori, A. D., Wylie, J. N., Munson, C., Zhu, Y. et al. (2011). Chromatin remodeling complex dosage modulates transcription factor function in heart development. *Nat. Commun.* **2**, 187.

Verzi, M. P., McCulley, D. J., De Val, S., Dodou, E. and Black, B. L. (2005). The right ventricle, outflow tract, and ventricular septum comprise a restricted expression domain within the secondary/anterior heart field. *Dev. Biol.* **287**, 437-449.

Yang, L., Cai, C. L., Lin, L., Qyang, Y., Chung, C., Monteiro, R. M., Mummery, C. L., Fishman, G. I., Cogen, A. and Evans, S. (2006). Isl1Cre reveals a common Bmp pathway in heart and limb development. *Development* **133**, 1575-1585.

Zhang, S. S., Kim, K. H., Rosen, A., Smyth, J. W., Sakuma, R., Delgado-Olguin, P., Davis, M., Chi, N. C., Puviindran, V., Gaborit, N. et al. (2011). Iroquois homeobox gene 3 establishes fast conduction in the cardiac His-Purkinje network. *Proc. Natl. Acad. Sci. USA* **108**, 13576-13581.

Zhang, W., Chen, H., Wang, Y., Yong, W., Zhu, W., Liu, Y., Wagner, G. R., Payne, R. M., Field, L. J., Xin, H. et al. (2011). Tbx20 transcription factor is a downstream mediator for bone morphogenetic protein-10 in regulating cardiac ventricular wall development and function. *J. Biol. Chem.* **286**, 36820-36829.